PCCP

Stochastic and network analysis of polycyclic aromatic growth in a coflow diffusion flame

Journal:	*Physical Chemistry Chemical Physics*
Manuscript ID	CP-ART-07-2020-003529.R2
Article Type:	Paper
Date Submitted by the Author:	23-Dec-2020
Complete List of Authors:	Saldinger, Jacob; University of Michigan, Elvati, Paolo; University of Michigan, Mechanical Engineering Violi, Angela; University of Michigan,

PCCP

ARTICLE TYPE

Cite this: DOI: 00.0000/xxxxxxxxxx

Stochastic and network analysis of polycyclic aromatic growth in a coflow diffusion flame

Jacob Saldinger,[a] Paolo Elvati, [b] and Angela Violi*[a,b,c]

Received Date
Accepted Date

DOI: 00.0000/xxxxxxxxxx

An important step in predicting the growth of soot nanoparticles is understanding how gas phase variations affect the formation of their aromatic precursors. Once formed, these aromatic structures begin to assemble into nanoparticles and, regardless of the clustering process, the molecular properties of the aromatic precursors play an important role. Leveraging existing experimental data collected from a coflow Jet A-1 surrogate diffusion flame, in this paper we report on a detailed study of the spatial evolution of molecular structures of polycyclic aromatic compounds (PACs) and their corresponding formation pathways. To this end, we employed the SNapS2 kinetic Monte Carlo software to simulate the chemical evolution of PACs along multiple streamlines. The results show that growth only occurs along streamlines that traverse regions of high acetylene concentrations in the center of the flame. The PACs predicted in various conditions show diverse chemical properties, including aliphatic chains, five-membered, and heteroaromatic rings. PACs in streamlines close to the flame wings begin growing immediately due to the high temperature and large amounts of radical species, while PACs originating along inner streamlines do not appreciably grow until they pass through an area characterized by high radical concentrations. Using graph theory and network analysis, we investigated the complex reaction network generated by SNapS2 and determined that the growth pathways of many PACs center around a few stable structures that also promote oxygen addition reactions due to their morphology and long lifetimes. These pathways play a more significant role along streamlines near the centerline, compared to the flame wings, which show more variety due to the highly reactive environment encountered during early growth. The results of this study provide insights on the reaction pathways that determine the properties of PACs at different flame locations as well as information on the chemical characteristics of the formed PACs, with emphasis on oxygenated structures.

1 Introduction

For decades, polycyclic aromatic compounds (PACs) formed in flames have raised great interest, not only for their adverse health effects and negative impact on the environment[1], but also for their key role as nanoparticle and soot precursors[2].

There is a pressing need to link specific combustion environments (*i.e.*, temperature and composition of gas-phase species) to the properties and growth pathways of these molecules. Past studies have determined that factors such as fuel[3] and reaction conditions[4] influence the quantity and types of PACs formed. Because the high reactivity of combustion drives growth through a number of unique pathways, properly representing PACs in these dynamic processes poses a challenge. Traditional study of these compounds have focused on the stabilomer grid[5], a set of peri-condensed fused carbon molecules. Still, a number of features are not captured in these models including oxygen[6], curvature[7], and aliphatic branching[8] which have all been observed in various experiments.

With the goal of assessing the influence of combustion conditions on the growth pathways of PACs, in this work we study the molecular evolution of aromatic species along various streamlines of a coflow flame, using the kinetic Monte Carlo (kMC) SNapS2 code[9], previously developed by our group. The flame has been experimentally characterized by Cain *et al.* who identified a significant amount of oxygenated PACs and PACs with aliphatic components[10]. Starting from results that we have obtained comparing the PACs formed along the centerline of the flame with experiments [11], we expand the study to include the outer radial streamlines to assess the growth of PACs depends on spatial variation in the flame and analyze the results using graph theory and network analysis.

[a] *Dept. of Chemical Engineering, University of Michigan, Ann Arbor, MI, 48109 USA*
[b] *Dept. of Mechanical Engineering, University of Michigan, Ann Arbor, MI, 48109 USA*
[c] *Dept. of Biophysics, University of Michigan, Ann Arbor, MI, 48109 USA*
* *corresponding author avioli@umich.edu*

† Electronic Supplementary Information (ESI) available: species concentration profiles relative to streamlines. See DOI: 10.XX

As we have shown in the past in a counterflow ethylene flame, the PACs formed within different streamlines in the same flame can be vastly different[12]. To this end, we consider properties such as size, oxygenation, five-membered rings, and presence of aliphatic chains, which have all been shown to influence the propensity of PACs to grow into larger combustion nanoparticles[13–15]. We observe a diverse set of PACs and identify the structural and gas-phase characteristics leading to their formation. The results from this study highlight the relative importance of reaction pathways in the flame and provide information on the chemical characteristics, including oxygen content, of PACs.

2 Methodology

2.1 System

The coflow non-premixed diffusion flame employed in this study used a Jet A-1 surrogate mixture (72% *n*-decane, 18% propylbenzene, 10% propylcyclohexane by mass) as fuel. More details on this flame and surrogate can be found in[16]. For the temperature and concentrations of small gas-phase molecules needed by SNapS2, we used previously published computational fluid dynamics (CFD) data[16,17]. The surrogate blend and base kinetic mechanism used for this study was developed by Dagaut *et al.*[18] while the PAH growth mechanism developed by Slavinskaya *et al.*[19,20] was used to simulate larger molecules.

As we have previously proposed[12], the streamlines were determined by numerical integration of the velocities starting at a radial distance of 0.5, 2.5, 5, 7.5, 10, and 12.5 mm from the flame central axis (assuming cylindrical symmetry). Figure 1 shows the streamlines in relation to flame temperature and selected gas-phase species.

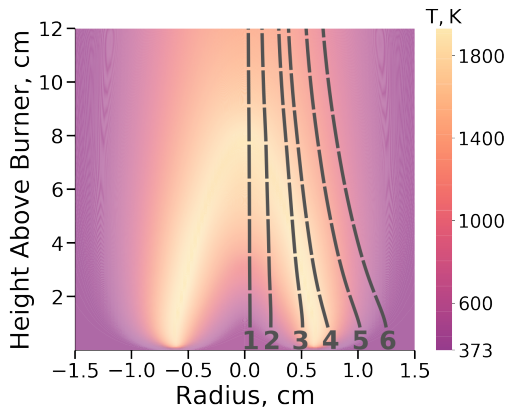

Fig. 1 Temperature profile of the coflow diffusion flame from CFD data published by Saffaripour and coworkers[17]. Streamlines considered in this work are shown as dark lines.

2.2 Stochastic Simulations

Stochastic simulations were performed using SNapS2[9,12] a kMC software that generates a large number of PAC growth histories (structure and lifetime). SNapS2 considers the small molecule gas-phase environment to produce the time resolved chemical evolution of selected molecules (seeds) through a set of stochastically selected generic reactions. We refer to these reactions as generic because they are not associated to a given molecule but rather to a specific chemical group. By using this approximation, SNapS2 is better able to simulate the formation of a large number of species.

The current SNapS2 mechanism used in this study has 394 unique generic reactions. The mechanism is built upon the one described by Wang *et al.*[12], with the addition of reactions that describe the formation of ketones[21], furans[22], aliphatic chains[23], five-membered rings[24], and ring oxidation[25].

Concentration profiles of temperature and selected small gas-phase species used as inputs into our simulations are taken from Saffaripour *et al.*[16] and shown in the supporting information. Concentrations between data points were approximated using spline interpolation in SciPy[26]. While there are some discrepancies between the concentrations of small gas-phase species calculated in CFD and measured experimentally,[16] these deviations are unlikely to significantly affect the outcome of our work. As discussed elsewhere,[27] similar level of inaccuracies of the gas-phase do not stop our model from quantitatively reproduce experimentally observed PAC properties[12], likely due to the comparatively large rates of competing reactions.

As starting points of SNapS2 histories, we considered a pool of seed molecules used in[11] that includes cyclopentadiene, cyclopentadienyl, benzene, phenyl, toluene, napthalene, phenol, phenolate, phenanthrene, and acenaphthylene. Since the statistical importance of each history depends on the concentration of the starting molecule (seed), any molecule among the selected pool that at any point had a concentration of at least 5% of the maximum concentration of C_6H_6 (the highest concentration seed molecule in all streamlines) was simulated in each streamline. Seed molecule concentration profiles are provided in the supporting information. The simulations for all molecules were started at intervals of 5 ms, which was then shortened to 1 ms when each molecule's concentration was above the 5% threshold. For efficiency reasons, we stopped our simulations when the PAC either reached 600 u (the upper mass in previous experimental[10] and computational[11] studies of this flame) or reached the end of our flame system. For each time origin, we performed 100 simulations for the seed with the highest concentration (C_6H_6 in all streamlines) and, for the other species, a number of simulations based on their relative concentration. Overall, we simulated the growth history of approximately 30,000 molecules. We observed approximately 6 million unique species (including radicals) and 6.5 million unique reactions, defined as a reaction with a unique reactant and product.

2.3 Reaction Network Analysis

For our study of formation pathways, we conducted a graph analysis of our results by creating a graph where each node is represented by a unique species and each edge is a unique reaction. In this representation, each molecular growth history is described by a directional graph. Graph analyses are performed with the Networkx library[28].

3 Results and Discussion

3.1 Validation

As first step in our study, we consider the comparison between between the results from SNapS2 and the experimental data[10] along the centerline of the flame.

Figure 2 shows a comparison of oxygen and carbon numbers for compounds sampled at a height of above the burner (HAB) of 50 mm. The open triangles represent the simulations results, the open circles are the experimental data, and the filled crosses indicate a match between modeling and experiments. Overall, our simulations reproduce well the experimental O/C content over a wide mass range but fail to capture a few highly oxygenated species at low carbon numbers. However, based on the oxygen-carbon ratios we suspect that these structures are not PACs but rather aliphatic in character, for which the current kinetic mechanism used in SNapS2 is incomplete. We also predict a few highly oxygenated species with high carbon numbers not seen in experiments, but since we sampled over an order of magnitude more structures than the experiment (approximately 10000 *vs* 500) it is possible that some, if not all, of these points represent less common structures that were missed due to limited sampling. Also as discussed elsewhere[11,14], other phenomena such as physical dimerization and radical–radical reactions may remove heavy PACs from the system as they form large molecular clusters. Of note, our simulations produce significant amounts of unoxygenated PACs that were not included in this comparison as the experimental technique did not allow for the measurement of these compounds. For this reason, we omit unoxygenated PACs from this comparison, however, we include these PACs in all subsequent analyses. In addition to these aromatic precursor molecules, Cain *et al.* also observed a number of large aliphatic components and soot particles at higher flame heights[10]. As the SNapS2 mechanism and seed molecules focuses on aromatic growth, these molecules were not captured in our PAC analysis. Additional comparisons between our modeling methodology and experiments at other heights in the flame along the centerline are reported elsewhere[11], and show similar results.

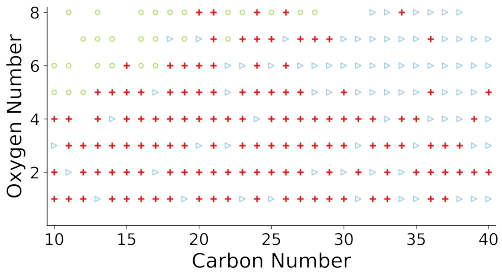

Fig. 2 Number of oxygen atoms vs. number of carbon atoms observed along the centerline at HAB=50 mm. Green open circles are experimental observations from[10]. Blue open triangles are molecules from our simulations. Red filled crosses are agreement between simulation and experiment.

3.2 Composition and size spatial dependence

Of the six streamlines we considered, PACs growth was only observed on the inner three (labeled 1,2, and 3 in Fig. 1). This result can be explained by looking at the acetylene concentration (see Supplementary Material) because only the three streamlines closest to the center pass through the acetylene rich region. Of note, the streamline number 4 goes through a region with a high concentration of radicals (mostly H, O, OH and CH_3) but we do not observe any relevant growth, showing again that acetylene is the most critical species for PAC growth[29,30]. Since only the three internal streamlines (1 to 3) show significant growth, in the following we will focus only on those streamlines.

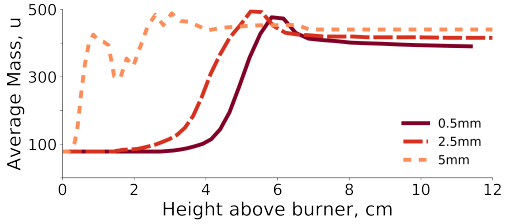

Fig. 3 Average mass vs. HAB along the three streamlines.

Figure 3 reports the evolution of the average PAC mass (weighted by PAC lifetime and species concentration) along streamlines 1–3. As expected based on the lack of growth in the outer streamlines, PACs experience their fastest growth when they pass through the high temperature, radical rich section in the flame. After traveling through this region, the gas-phase environment is less conducive to PAC growth as the average PAC mass remains the same or slightly decreases. As our model does not consider the aggregation of PACs, it is likely that at higher HABs the average mass of the PACs may be lower than the one predicted in Figure 3 as heavier PACs may aggregate into larger soot particles[10]. While mass provides a first characterization of PAC growth, in order to understand the diversity of the PACs formed in distinct regions, we need to study the molecular chemical characteristics, *i.e.*, oxygen content, presence of five-membered rings and aliphatic chains.

We first analyzed how oxygen content varies between and along different streamlines in Fig. 4. Streamline number 3 (r=5 mm) starts in a highly reactive region in the flame wing and begins growing immediately, while the other two exhibit minimal oxygenation prior to reaching a similarly reactive environment.

The most interesting aspect however, is the fact that the trend in the average oxygen content among the streamlines matches the one observed in the mass growth. This is one additional proof of previous findings[14,27] which observed that the oxygenated species feature prominently in the early growth of PACs. In contrast to scenarios where PACs undergo oxygen addition reactions[27], here we do not observe separate regions favoring PAC growth through oxygen addition reactions and carbon addition reactions. In this flame, the gas-phase conditions where reactions involving the addition of carbon atoms and the addition of oxygen atoms are favorable, are the same.

The analysis of the types of oxygenated chemical groups shows

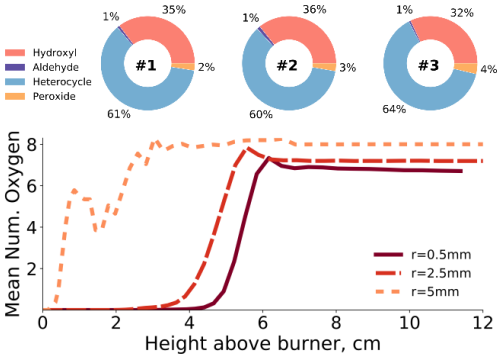

Fig. 4 Oxygen atoms in the PACs' structures in each of the 3 inner streamlines: mean number of oxygen atoms per PAC at different HABs (bottom) and analysis of the distribution of oxygen containing functional groups near the peak oxygen content of each streamline (top). Functional groups were sampled over a range of 5 mm centered at 62 mm, 56 mm, and 30 mm for streamlines number 1, 2, and 3, respectively.

a large prevalence of furans and hydroxyls, followed by small amounts of peroxides formed by the reactions with HO_2 radicals. Aldehydes make up an almost negligible percentage of the groups, which is consistent with another work[31] that suggests they play a larger role in the post-flame region. We observe only trace amounts of ethers. The comparison between the streamlines shows a slight increase of furan and peroxide groups when moving away from the centerline. We attribute the latter to a 10-times higher peak concentration of HO_2 and a lower temperature in the areas of high HO_2 concentration, which slows the peroxide decomposition rate[32].

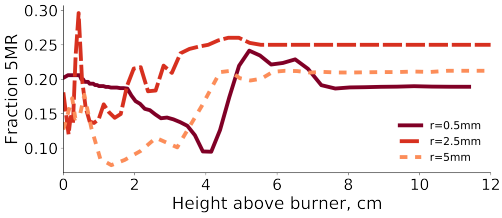

Fig. 5 Fraction of five-membered carbocycles as a function of HAB.

Previous studies of this[11] and other flames[33,34] show that five-membered aromatic carbon rings are a common group in these PACs. Here, we study how the fraction of five-membered carbon rings, defined as the total number of five-membered carbon rings divided by the total number of five and six-membered carbocycles in the PAC ensemble, varies along and between streamlines. The analysis of these streamlines confirms that five-membered carbon rings constitute an important structural feature of PACs in this flame as we observe a 10% to 30% fraction across all streamlines (Fig. 5). While in some measure, particularly at very low heights above the burner, the concentration of seed molecules affects the value (*e.g.*, benzene *vs.* cyclopentadiene), the evolution of this fraction provides useful insights into the mechanisms of growth.

Early in all streamlines, the fraction of five-membered rings decreases as the PACs begin to grow. While the number of five-membered carbocycles is still increasing in this region (albeit slowly), the six-membered ring growth is occurring much more rapidly. This is consistent with known chemistry as six-membered rings can grow from a variety of pathways and active sites involving the edges of aromatic rings[4]. Later in the flame however, large PACs possess more zigzag sites[35] which have been shown to be particularly amenable[36] to the growth of five-membered carbon rings. Thus, while edge growth is always favorable for six-membered rings, five-membered carbon ring growth does not become favorable until larger PACs exist in the system and more of these zig-zag sites are available. Examining the effect of these five-membered rings on shape, figure 6 shows that compared to those with only six-membered rings, structures with five-membered rings can exhibit significant curvature although this is not necessarily the case.

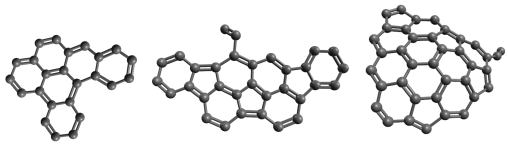

Fig. 6 Left: A planar PAC with only six-membered rings. Center: A planar PAC with five and six-membered rings. Right: A curved PAC with five and six-membered rings.

Numerous studies[8,37] suggest carbon chain growth occurs on PACs in flames. Thus, we conclude our PAC structural analysis describing the aliphatic components of PACs (not to be confused with purely aliphatic molecules). The majority of carbons within our simulated PACs are members of rings or sp^2 hybridized, indicating there is very little non-aromatic branching. Still, notable exceptions do exist.

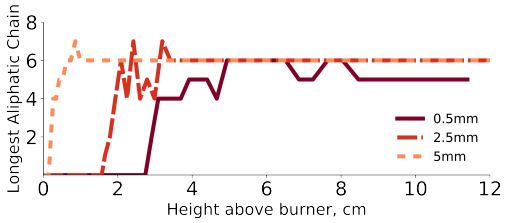

Fig. 7 Length of longest aliphatic chain along each streamline.

Figure 7 shows the longest observed aliphatic chain on each streamline at each HAB. These carbon chains begin to be observed just as each streamline starts to enter the high temperature region of the flame. In these sections of the flame, the temperature is high enough for PAC growth reactions to occur, however, the streamline has yet to reach its maximum temperature. This behavior supports past work[38], which has hypothesized that aliphatic growth is most prevalent at elevated temperatures but not at the highest temperature section of the flame. As indicated in figure 7, the maximum chain length does not appreciably change after its initial growth even as the streamlines pass through the highest temperature, highest radical concentration section of the flame. This suggests that these side chains have a degree of stability and do not necessarily break down even in the most reactive environments of this system. The presence of

aliphatic chains can be also dictated by some characteristics of the PACs' structures that are conducive to the growth of these chains. To test this hypothesis, we identified only those growth histories in which an aliphatic chain of at least five carbons is formed and analyzed the structure of the first PAC molecule in the history that had this aliphatic chain. Although we observe no unifying feature (two examples of the variety of structures can be seen in Fig. 8), we most commonly observe PACs between 30 and 35 carbons, including the aliphatic chain. Based on some of the observed structures (such as Fig. 8) it appears many of the aliphatic chains form when a smaller carbon chain is unable to close into a ring. Thus, it follows that more aliphatic chains grow on PACs in this size range as they require a particular growth site which is more likely to exist on larger PACs.

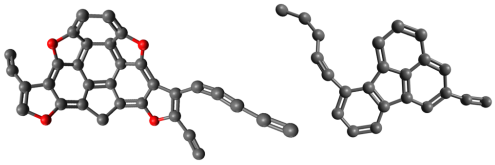

Fig. 8 Two examples of observed molecules with aliphatic chains.

While these long hydrocarbon chains are not observed in high concentrations, numerous studies[13,39,40] have suggested these compounds can play a role in the physical growth of PACs into combustion nanoparticles. The early growth of these branched PACs and their long lifetimes within the flame suggest that despite being minor species they can still contribute to PAC aggregation, by stabilizing the formation of PACs aggregates long enough for them to form a chemical bond for example by radical-radical reactions[14,41].

3.3 Reaction Network Analysis

The ensemble of stochastic simulations generated by SNapS2 can be used to study the growth pathways of PACs and how they are affected by the conditions inside the flame. Due to the generic nature of the reactions in the SNapS2 mechanism, we are particularly interested in identifying which PAC substructures are associated with growth and any differences arising from varying environments. This analysis is complicated by (1) the large number of highly reversible reactions and (2) the fact that independent reactions can happen on separate locations of larger molecules. The two problems are intertwined (as reversible reactions can happen on different atoms) and an analysis of the growth histories show that, on average the ratio between the total number of species and reactions simulated in a single growth history and the number of unique species and unique reactions (as defined in section 2.2) in a growth history are about 40 and 20, respectively. For this reason, we transformed the ensemble of histories into graphs as described in the Methodology section. In this analysis, each growth history is represented by an unweighted directional graph, with weights between each graphs determined by the initial concentrations of their seed molecules. We defined the shortest path between the first and final molecules of each simulation as the formation pathway. Shortest paths are not necessarily the only pathway of growth of each molecule, but rather a basic description of common, multi-step growth pathways, which has been shown to be useful in deterministic reaction network analyses[42]. To identify the shortest paths, we used Dijkstra's algorithm[43].

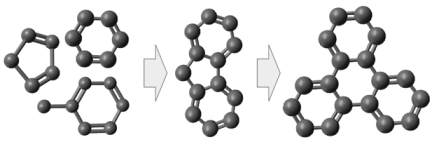

Fig. 9 Simplified description of the formation pathway to commonly observed 18 carbon PAC. Single ring molecules (left) grow into a 13 carbon molecule resembling fluorene (center). A cyclopentenyl is then added to form an 18 carbon PAC (right).

If we analyse the reaction sequences in the shortest paths, all three streamlines seem to follow a prevalent carbon pathway for early growth. Almost all single ring aromatics (approximately 85% in all streamlines) grow into a 13 carbon atom consisting of a structure similar to fluorene (Fig. 9, center structure). Although most of this growth occurs through hydrogen abstraction acetylene addition (HACA)[29], we observe some C_6H_6 also form these 13 carbon structures by adding an oxygen and disassociating a CO. Polycyclic aromatic seeds such as napthalene and phenanthrene form this 13 carbon structure in a smaller amount as there are more active sites to grow in other directions early in the growth history and transitioning to the fluorene-like structure requires significantly more molecular rearrangement. In the streamlines 1 and 2, approximately 50% of all pathways forming these 13 carbon structures then add a cyclopentenyl radical to form an 18 carbon structure resembling triphenylene (when unoxygenated) using a reaction similar to the one described in[44]. This species has been experimentally observed as a polycyclic aromatic hydrocarbon in other combustion systems[45]. In the outer streamline (number 3) this sequence of reactions still occurs but in a smaller amount (approximately 30%). This pathway along with HACA and oxygen additions comprise almost all the growth in this region for all streamlines.

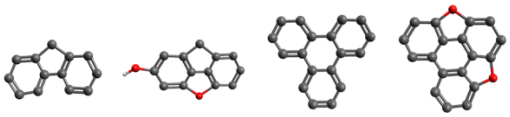

Fig. 10 Some commonly observed 13 carbon (left 2) and 18 carbon (right 2) structures along the center (1) streamline.

The two structures described above also appear integral to the formation of oxygenated PACs. As shown in Figure 10, oxygen addition occurs through the addition of furans to the four carbon armchair sites these molecules possess. Furthermore, as these are some of the most common molecules we observe in our simulations, this suggests they are stable and exist for relatively long times within the flame. Thus it appears these structures promote additions of oxygen both through offering a favorable armchair site for furan formation and by ensuring that the probability of oxygen reactions occurring on these structures is much higher owing to their long lifetimes.

While these reaction pathways are present in a significant number of the traces analyzed, they are by no means the only growth reactions. Thus, we also expand our network analysis to consider the relative importance of every reaction observed in our simulations. For each streamline, we combined all individual traces to create a single directed graph, as described in the Methodology section. To obtain the relative frequency at which each reaction occurs, edges were weighted by the initial seed molecule concentration as well as the net difference in occurrences between the forward and reverse reactions. Since we observed approximately 6 million unique molecules and many of these PACs exhibit similar structures (e.g. differ by a hydrogen atom), we grouped molecules sharing carbon number, oxygen number, number of six-membered rings, number of five-membered rings, and number of furans and then represented each reaction group with the most frequently observed pair of molecules (based on the above weights) for the purpose of our analysis. For each streamline graph, we considered the edges with the highest weights as the most commonly observed reactions. While we included all reactions in our graph, we omitted single ring structures from subsequent analysis. We instead focused on polycyclic molecules as single ring reactions are well accounted for in the deterministic mechanism[18] and dominate all other PAC growth reactions in frequency due to the high concentration of single ring seed molecules and the fact that there are significantly fewer active sites and thus fewer possible growth pathways relative to other species. The top fifteen most frequently observed unique reactions for each streamline along with their relative weights are shown in the Supplementary Material in Figs. S9-S11.

For all three streamlines, our analysis identifies a diverse set of reactions playing an important role in PAC growth including acetylene additions, oxygen additions, and ring closures. We observed reactions involving the 13 carbon (e.g. reactions **1.2**, **2.2**, and **3.5**) and 18 carbon PACs (e.g. reactions **1.10** and **2.12**) also identified by our shortest path analysis, confirming that these molecules appear frequently in growth reactions. Some of the highest weighted reactions across all streamlines involve the addition of two acetylene molecules to indene through HACA (reactions **1.1**, **1.3**, **2.1**, **2.3**, **3.2**, and **3.14**) then a subsequent ring closure to form a fluorene-type molecule (reactions **1.2**, **2.2**, and **3.5**) showing the importance of this structure to PAC growth in this flame. Furthermore, all streamlines show reactions involving the addition of an oxygen to this fluorene-type molecule (reactions **1.8**, **2.5**, **3.4**, **3.8**, **3.10**, and **3.13**) validating the importance of this PAC to oxygen addition reactions as discussed above. We also observe a number of influential reactions involving species other than the ones considered in our above shortest pathway analysis. Most notably, in streamlines 1 and 2 we see acenaphthylene grow through HACA reactions (reactions **1.4**, **1.5**, **2.4**, and **2.9**) to form a 16 carbon PAC consisting of a five-membered ring surrounded by three six-membered rings (reactions **1.7** and **2.6**). This structure is of particular interest as it subsequently can form a PAC characterized by an embedded five-membered ring which in other flames has been noted to contribute to molecular curvature[46]. This structure also commonly participates in oxygen addition reactions (reactions **1.14** and **2.14**). The omission of this 16 carbon structure and these growth reactions shows one possible limitation of our shortest path analysis. Since that analysis considers the pathway with the least number of reactions, when considering growth pathways for PACs with a carbon number between 13 and 18, the analysis likely somewhat overweighs the growth contribution of the addition of the cyclopentenyl radical relative to HACA growth as the former reaction achieves more mass growth with fewer reaction steps. Thus, traditional HACA growth pathways and their resulting molecules also appear highly relevant at these mass ranges.

In all our previous analyses, we have described mostly commonalities among the different streamlines, species, and reaction pathways. Overall, we find that, compared to counterflow flames[12], this flame shows less variations in the characteristics of the formed PACs. There are however some interesting differences, especially in the types of oxygenated PACs. As shown in Figs. S9-S11, streamlines 1 and 2 show similar types of reactions compared to streamline 3. The most commonly observed reactions in streamlines 1 and 2 show significantly fewer oxygen addition reactions with 2 and 3 oxygen addition reactions respectively compared to 8 reactions for streamline 3, including two of the top 3 reactions. In addition, the PACs in streamline 3 have a significantly higher oxygen content than the most commonly observed reactions in the other two streamlines. In streamline 3 all but three of the top fifteen most influential reactions involve at least one oxygenated PAC. While some of these trends can be explained by the higher concentration of small oxygenated aromatics such as phenol in streamline 3 relative to the other streamlines, much of this is due to the higher amount of reactions involving the addition of oxygen, which occur in streamline 3 at lower carbon numbers relative to streamlines 1 and 2. The reactions observed in Figs S9-S11 involve PACs with carbon numbers between 9 and 22 carbons. Thus, the fact that the average oxygen content is similar across all streamlines at higher HABs (Fig. 4) suggests that reactions involving the addition of oxygen atoms to PACs occur more frequently at lower carbon numbers in streamline 3 and at higher carbon numbers in streamlines 1 and 2.

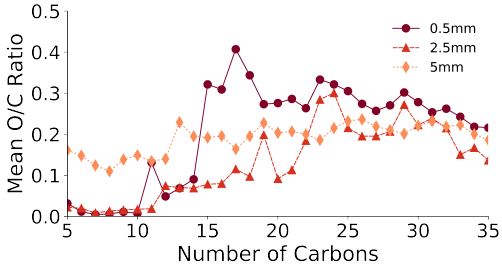

Fig. 11 Oxygen-carbon ratios for different carbon numbers along each streamline.

This trend can be further seen in how the oxygen content of PACs vary with size. Figure 11 shows the average number of oxygens (weighted by lifetime and seed molecule concentration) on PACs of each carbon number. The streamline number 1 (r=0.5 mm) has two different PACs groups: one, with less than 13 carbons, showing very little oxygenation (consistent with fig-

ure 10) and one, with higher mass, showing significant oxygenation. The next streamline moving outwards (r=2.5 mm, still not in the wing) shows a similar trend albeit with generally a smaller relative amount of oxygenation particularly for PACs up to 22 carbons. The third streamline (r=5 mm) in which we observe early growth and the one that is in the flame wing, breaks the trend, showing a near constant oxygen-carbon ratio.

These results suggest that the PACs in the streamlines closer to the center follow a growth pathway where carbon additions occur prior in molecular growth history to significant oxygen additions while in streamline 3, oxygen and carbon addition reactions occur at all phases of the PAC growth history. This difference is compatible with the acetylene and radicals concentrations along each streamline (see Supplementary Materials). Early in the flame, streamline 3 experiences high concentrations of radicals and C_2H_2 for an extended period of time in close proximity: although the concentration of C_2H_2 and radicals peak in different locations, the C_2H_2 concentration is within one order of magnitude of its maximum value while the radical concentration peaks. Both of these are necessary for HACA reactions[30] but at the same time the O, OH, and HO_2 radicals promote oxygen addition reactions[9]. The innermost streamlines, however, pass through the region of high radical concentration after the C_2H_2 rich area where radicals have a moderate concentration.

4 Conclusion

Using the SNapS2 kinetic Monte Carlo software, we studied spatial variations in the properties of polycyclic aromatic compounds and their formation pathways as they travel in a Jet A-1 diffusion flame. The results show a growth generally matching the temperature, acetylene, and radical species profiles: PACs begin growing almost immediately in the wings but do not grow in the center of the flame until higher HABs are reached.

Of note, PACs in the outer part of the wings (or farther away) experience negligible growth despite going through a high temperature region. Although similar in average mass, PACs in the inner part of the flame experience the formation of oxygenated groups (mostly hydroxyls, heterocycles, and peroxides) later on, once larger PAHs are formed. The differences in the growth histories are also reflected in an increase in five-membered rings, heterocycles, and peroxides and a slight decrease in hydroxyl groups when moving away from the flame center.

Finally, through a network analysis of the growth histories, we identified some common symmetrical structures (between 10 and 20 carbons) that are formed both via HACA mechanisms and oxygen mediated reactions.

Acknowledgements

The Authors thank Prof. P. Dagaut for providing the kinetic mechanism and Prof. M. Thomson for the data on the small gas-phase species computed in the coflow flame. This work is supported in part by the U.S Department of Transportation, FAA Center of Excellence 13-C-AJFE-GIT-067, the U.S. Army Research Office under grant No. W911NF-14-1-0359 and by the College of Engineering (BlueSky) at the University of Michigan.

Notes and references

1 W. Wang, N. Jariyasopit, J. Schrlau, Y. Jia, S. Tao, T. Yu, R. Dashwood, W. Zhang, X. Wang and S. Simonich, *Environ. Sci. Technol.*, 2011, **45**, 6887–6895.
2 A. D'Anna, *Proc. Combust. Inst.*, 2009, **32**, 593–613.
3 S. Choi, B. Choi, S. Lee and J. Choi, *Exp. Therm. Fluid Sci.*, 2015, **60**, 123 – 131.
4 H. Richter and J. Howard, *Prog. Energ. Combust.*, 2000, **26**, 565–608.
5 S. Stein and A. Fahr, *J. Phys. Chem.*, 1985, **89**, 3714–3725.
6 K. O. Johansson, T. Dillstrom, M. Monti, F. El Gabaly, M. Campbell, P. Schrader, D. Popolan-Vaida, N. Richards-Henderson, K. Wilson, A. Violi and H. Michelsen, *Proc. Natl. Acad. Sci.*, 2016, **113**, 8374–8379.
7 A. Abdalla, Y. Ying, B. Jiang, X. He and D. Liu, *J. Energy Inst. (in press)*, 2019, 62 – 75.
8 M. Commodo, K. Kaiser, G. De Falco, P. Minutolo, F. Schulz, A. D'Anna and L. Gross, *Combust. Flame*, 2019, **205**, 154–164.
9 Q. Wang, P. Elvati and A. Violi, *In Preparation*, 2020.
10 J. Cain, A. Laskin, M. Kholghy, M. Thomson and H. Wang, *Phys. Chem. Chem. Phys.*, 2014, **16**, 25862–25875.
11 J. Saldinger, Q. Wang, P. Elvati and A. Violi, *Fuel*, 2020, **268**, 117198.
12 Q. Wang, P. Elvati, D. Kim, K. O. Johansson, P. E. Schrader, H. A. Michelsen and A. Violi, *Carbon*, 2019, **149**, 328–335.
13 S. Chung and A. Violi, *Proc. Combust. Inst.*, 2011, **33**, 693–700.
14 P. Elvati, V. Dillstrom and A. Violi, *Proc. Combust. Inst.*, 2017, **36**, 825–832.
15 P. Elvati, K. Turrentine and A. Violi, *Proc. Combust. Inst.*, 2019, **37**, 1099–1105.
16 M. Saffaripour, A. Veshkini, M. Kholghy and M. Thomson, *Combust. Flame*, 2014, **161**, 848–863.
17 M. Saffaripour, M. Kholghy, S. Dworkin and M. Thomson, *Proc. Combust. Inst.*, 2013, **34**, 1057–1065.
18 P. Dagaut and S. Gaïl, *J. Phys. Chem. A*, 2007, **111**, 3992–4000.
19 N. Slavinskaya and P. Frank, *Combust Flame*, 2009, **156**, 1705 – 1722.
20 N. Slavinskaya, U. Riedel, S. Dworkin and M. Thomson, *Combust Flame*, 2012, **159**, 979 – 995.
21 X. Zhong and J. Bozzelli, *J. Phys. Chem. A*, 1998, **102**, 3537 – 3555.
22 X. Shi, Q. Wang and A. Violi, *Combust. Flame*, 2020, **212**, 216 – 233.
23 H. Richter, S. Granata, W. Green and J. Howard, *Proc. Combust. Inst.*, 2005, **30**, 1397 – 1405.
24 A. Mebel, Y. Georgievskii, A. Jasper and S. Klippenstein, *Faraday Discuss*, 2016, **195**, 637 – 670.
25 M. Frenklach, Z. Liu, R. Singh, G. Galimova, V. Azyazov and A. Mebel, *Combust. Flame*, 2018, **188**, 284–306.
26 P. Virtanen, R. Gommers, T. E. Oliphant, M. Haberland, T. Reddy, D. Cournapeau, E. Burovski, P. Peterson, W. Weckesser, J. Bright, S. J. van der Walt, M. Brett, J. Wilson,

K. J. Millman, N. Mayorov, A. R. J. Nelson, E. Jones, R. Kern, E. Larson, C. J. Carey, İ. Polat, Y. Feng, E. W. Moore, J. VanderPlas, D. Laxalde, J. Perktold, R. Cimrman, I. Henriksen, E. A. Quintero, C. R. Harris, A. M. Archibald, A. H. Ribeiro, F. Pedregosa, P. van Mulbregt and SciPy 1.0 Contributors, *Nature Methods*, 2020, **17**, 261–272.

27 Q. Wang, J. Saldinger, P. Elvati and A. Violi, *Fuel*, 2019, **264**, 116773.

28 A. Hagberg, D. Schult and P. Swart, Proceedings of the 7th Python in Science Conference, Pasadena, CA USA, 2008, pp. 11 – 15.

29 M. Frenklach, D. Clary, W. Gardiner and S. Stein, *Symp. Combust.*, 1985, **20**, 887–901.

30 M. Frenklach, *Phys. Chem. Chem. Phys.*, 2002, **4**, 2028–2037.

31 J. Giaccai and J. Miller, *Proc. Combust. Inst.*, 2019, **37**, 903–910.

32 F. Battin-Leclerc, *Prog. Energ. Combust.*, 2008, **34**, 440 – 498.

33 R. Whitesides, D. Domin, R. Salomón-Ferrer, W. A. Lester and M. Frenklach, *J. Phys. Chem. A*, 2008, **112**, 2125–2130.

34 E. Yapp, C. Wells, J. Akroyd, S. Mosbach, R. Xu and M. Kraft, *Combust. Flame*, 2017, **176**, 172–180.

35 M. Frenklach, *Symp. Combust.*, 1996, **26**, 2285 – 2293.

36 R. Whitesides and M. Frenklach, *J. Phys. Chem. A*, 2010, **114**, 689–703.

37 K. Homann and H. Wagner, *Symp. Combust.*, 1967, **11**, 371 – 379.

38 H. Zhang, D. Hou, C. Law and X. You, *J. Phys. Chem. A*, 2016, **120**, 683–689.

39 P. Elvati and A. Violi, *Proc. Combust. Inst.*, 2013, **34**, 1837–1843.

40 K. Le, C. Lefumeux, P. Bengtsson and T. Pino, *Proc. Combust. Inst.*, 2019, **37**, 869–876.

41 K. O. Johansson, T. Dillstrom, P. Elvati, M. Campbell, P. Schrader, D. Popolan-Vaida, N. Richards-Henderson, K. Wilson, A. Violi and H. Michelsen, *Proc. Combust. Inst.*, 2017, **36**, 799–806.

42 P. Zhao, S. Nackman and C. Law, *Combust. Flame*, 2015, **162**, 2991 – 2998.

43 E. W. Dijkstra, *Numerische Mathematik*, 1959, **1**, 269–271.

44 Y. Murakami, T. Saejung, C. Ohashi and N. Fujii, *Chem. Lett.*, 2003, **32**, 1112–1113.

45 L. Zhao, M. Prendergast, R. Kaiser, B. Xu, U. Ablikim, M. Ahmed, B. Sun, Y. Chen, A. Chang, R. Mohamed and F. Fischer, *Angewandte Chemie International Edition*, 2019, **58**, 2–11.

46 Q. Wang, J. Saldinger, P. Elvati and A. Violi, *Proc. Combust. Inst. (in press)*, 2020, **39**, year.